Optimization of the Catalytic Activity of Ag@Cu2O Decorated on rGO for Organic Pollutant Degradation

Lei Chen , Shuang Guo , Eungyeong Park , Young Mee Jung *

Posted Date: 20 November 2023

doi: 10.20944/preprints202311.1196.v1

Keywords: Ag@Cu2O core-shell; rGO; 4-NP; chemical catalytic

Article

Optimization of the Catalytic Activity of Ag@Cu_2O Decorated on rGO for Organic Pollutant Degradation

Lei Chen [1], Shuang Guo [2], Eungyeong Park [2] and Young Mee Jung [2,3,*]

[1] School of Materials Science and Engineering, Jilin Jianzhu University, Changchun 130118, China; chenlei82@jlju.edu.cn
[2] Department of Chemistry, Institute for Molecular Science and Fusion Technology, Kangwon National University, Chunchon 24341, Korea.; guoshuang@kangwon.ac.kr; egpark@kangwon.ac.kr
[3] Kangwon Radiation Convergence Research Support Center, Kangwon National University, Chuncheon 24341, Korea
* Correspondence: ymjung@kangwon.ac.kr

Abstract: We successfully fabricated Ag@Cu_2O core-shell decorated on reduced graphene oxide (rGO) nanocomposites (ACRN) by a simple and convenient in situ substitution method. The properties of these ACRN with heterostructure layers were characterized by scanning and transmission electron microscopies and absorption spectroscopy. We used p-nitrophenol (4-NP) as a probe molecule to determine the chemical catalytic activity of the ACRN. Upon introduction of rGO, a high electron transfer efficiency was achieved; thus, the catalytic activity was improved significantly. Therefore, the ACRN exhibited significantly improved catalytic activity for the reduction of 4-NP and showed the high application value in the removal of toxic and harmful substances from water. In addition, the fabricated ACRN was used for the reduction of organic dyes and explosive pollutants to generate nontoxic products. Furthermore, the high charge redistribution and transfer among Ag, Cu_2O and rGO in the ACRN induced the high catalytic reduction of organic pollutants, indicating the excellent potential of these materials for applications in water pollution treatment.

Keywords: Ag@Cu_2O core-shell; rGO; 4-NP; chemical catalytic

1. Introduction

Recently, as a result of industrial development, environmental pollution by nitro compounds in water has become increasingly serious, attracting widespread attention from all sectors of society [1,2]. 4-Nitrophenol (4-NP) and other phenolic pollutants are the most representative pollutants in industrial wastewater [3,4]. The carcinogenic and mutagenic and pose a considerable threat to the environment and human [5,6]. Catalytic hydrogenation has the advantages of being simple and resulting in less environmental pollution during the treatment of phenolic pollutant compounds. This method has potential development prospects. At present, the key to the catalytic hydrogenation process for treating nitrophenol compounds is to develop efficient, stable, and low-cost catalysts. Therefore, many kinds of inorganic catalysts have been designed and fabricated for the catalysis of phenolic pollutants [7–10].

Traditional catalysts include noble metals (such as Pt, Pd, Au, and Ag) were widely used in 4-NP catalytic hydrogenation [11–14]. These catalysts exhibit high catalytic activity under mild reaction conditions. Extensive studies on these types of catalysts have been conducted worldwide. However, the challenge is to develop a new type of catalyst that is stable, highly active, and reusable. Therefore, metal/semiconductor composites were developed. The interface of the metal/semiconductor heterojunctions has outstanding advantages in catalytic applications. Due to the strong interaction between metal and semiconductor at the interface, charge transfer (CT) and transfer between the components in the composite region are the main features leading to significant changes at the heterojunction interface. More importantly, the stability of the nanocomposite is better than that of

 doi:10.20944/preprints202311.1196.v1

the individual components. In addition, to change the morphology, composition, and geometric structure of the material, the researchers can easily control the catalytic properties. Metal/semiconductor composites are excellent functional materials and are widely used in various materials [15–18]. In addition, core-shell nanostructures have been designed and fabricated to solve the problems of a single mechanism and limited material properties [19,20]. Therefore, Ag@Cu_2O nanoparticles were used for the chemical catalysis of phenolic pollutants. The difference in energy between Ag nanoparticles and Cu_2O induces electron transfer between the core and shell [21,22].

Two-dimensional (2D) materials show extraordinary mechanical, optical, electronic, and thermal properties, enabling expansion of their applications. Graphene, because of its high charge carrier mobility, has demonstrated excellent performance and has received extensive research attention since 2004, when it was developed as a novel 2D material [23,24]. The mechanical and electronic properties of monolayer or multilayer 2D graphene have made it a hot research topic in nanoelectronics. Therefore, graphene was widely used in the different catalysis systems. Graphene is also widely used in batteries, supercapacitors, solar cells, detectors, and sensors due to its excellent performance [25,26]. Ag@Cu_2O core-shell decorated on reduced graphene oxide (rGO) nanocomposites (ACRN) exhibited excellent catalytic activity because of the Cu_2O shell was in-situ growing on the Ag-rGO surface. After the introduction of rGO onto the Ag@Cu_2O core-shell, the material exhibited excellent catalytic performance and carrier transport [20].

In this study, ACRN were fabricated for catalytic studies. Ag-rGO nanocomposites were synthesized throw the sol-gel method, and Ag@Cu_2O nanocomposites were obtained by reducing cupric nitrate ($Cu(NO_3)_2$) in the presence of the hydrazine hydrate (N_2H_4). By tuning the concentration of $Cu(NO_3)_2$, the thickness of the Cu_2O shell of the Ag@Cu_2O can be controlled. These materials exhibited different catalytic properties and are expected to solve water pollution problems. The number of available free electrons increased, causing the catalytic target to randomly adsorb ACRN. More importantly, the ACRN show the high adsorption capacity, thus, the catalytic activity for 4-NP, methyl orange (MO), and trinitrophenol (TNP) were improved significantly.

2. Experimental section

For experimental details, please refer to the supplementary information.

3. Results and discussion

3.1. Morphological characterization of the ACRN

To obtain ACRN, we first fabricated Ag decorated on rGO (Ag-rGO) using the wet chemical method (Figure 1A). The Ag on the rGO acted as a nucleation site for the Cu_2O shell coating. By decreasing the volume of the Ag-rGO composite solution, the density of the Ag@Cu_2O decorated on the rGO was significant increase. Meanwhile, the size of the Ag@Cu_2O spheres increased significantly with the increase of the Cu_2O shell thickness. SEM images were obtained to characterize the morphology of the ACRN. As shown in Figure 2, after surface modification, the composite material maintained the 2D structure of rGO and spherical nanoparticles was arranged on the surface, indicating the successful fabrication of Ag@Cu_2O composites on the rGO platform. To confirm the core-shell structure, we obtained TEM images. As shown in Figure 3, the composites (Figure 3 B-D) we fabricated possessed a clear Ag-Cu_2O core-shell structure decorated on the rGO substrate. Figure 3A shows Ag decorated on the rGO substrate. By introducing 15 mL of Ag-rGO composite, Cu_2O formed and covered the Ag core. However, the Ag core was not fully covered by the Cu_2O shell (ACRN-1, Figure 3B). As the volume of the Ag-rGO composite decreased, the thickness of the Cu_2O shell increased significantly, resulting in complete coverage of the Ag core (ACRN-2 and ACRN-3, Figure 3C and 3D). Comparative observation showed that as the amount of Ag-rGO composite decreased, the shell thickness of Cu_2O also gradually increased until the thicknesses were approximately 18 nm (ACRN-2) and 30 nm (ACRN-3). Therefore, by controlling the amount of Ag-rGO composite and then controlling the thickness of the composite shell, composites with different structural properties were prepared. In the TEM images, we observed that the surface of the Cu_2O

Preprints (www.preprints.org) | NOT PEER-REVIEWED | Posted: 20 November 2023 doi:10.20944/preprints202311.1196.v1

shell was rough and porous, making the material conducive to molecular adsorption. Because of the loose structure on the surface of Cu_2O, the catalytic and active sites were increased for catalytic reduction of the target.

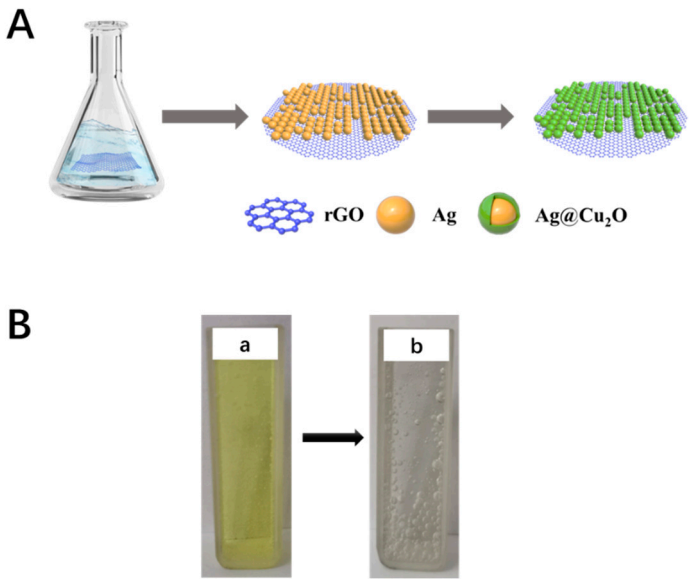

Figure 1. (A) Schematic of the preparation of the ACRN. (B) Optical photos of the reduction of 4-NP using the ACRN-2.

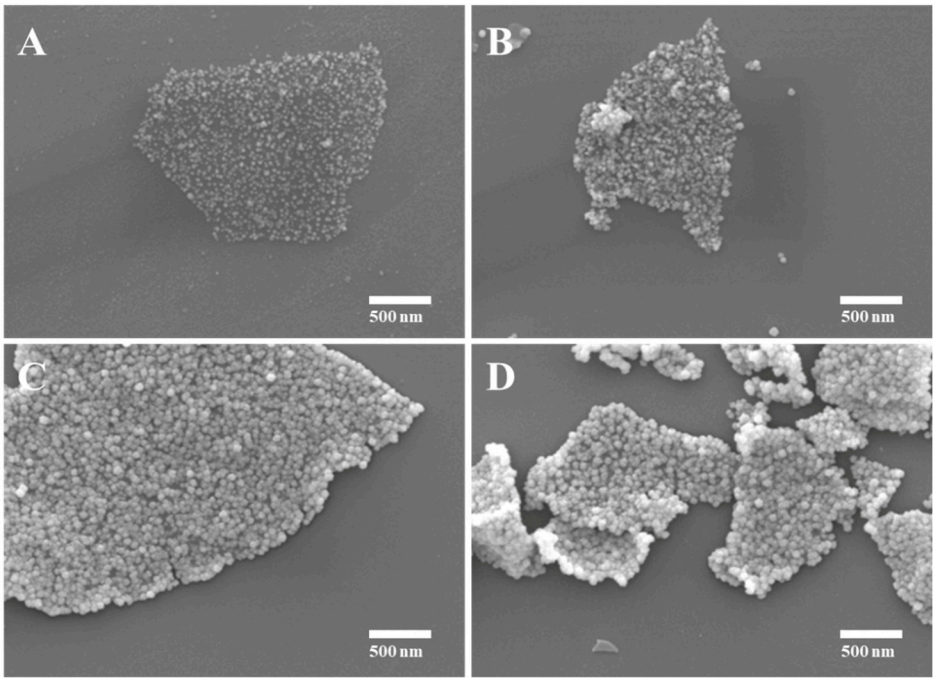

Figure 2. SEM images of Ag-rGO (A) and ACRN with different thicknesses of the Cu_2O shell (B-D).

Preprints (www.preprints.org) | NOT PEER-REVIEWED | Posted: 20 November 2023 doi:10.20944/preprints202311.1196.v1

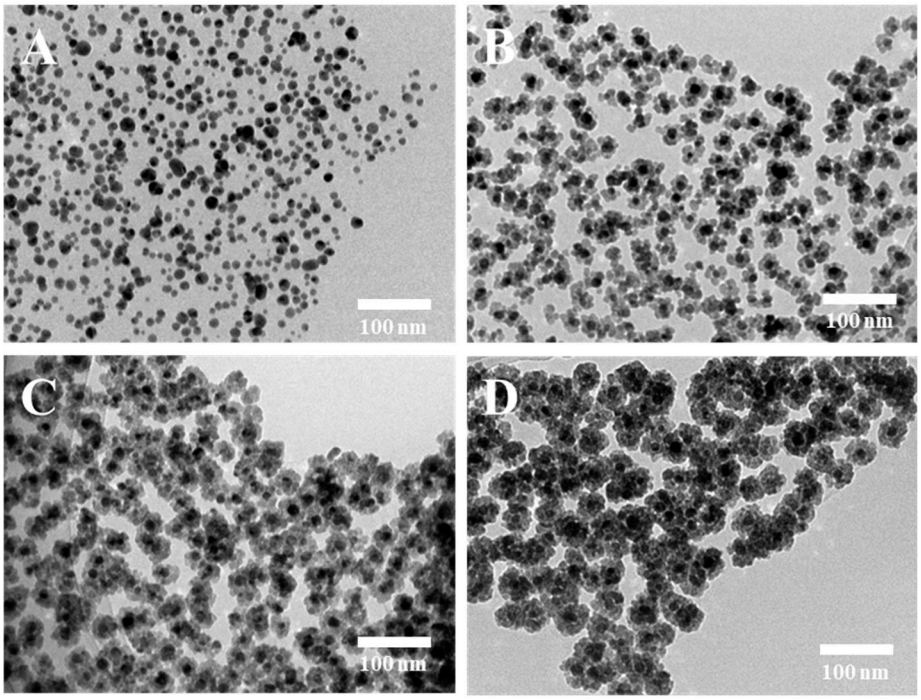

Figure 3. TEM images of Ag-rGO (A) and ACRN with different thicknesses of the Cu_2O shell (B-D).

To study the light response of the different ACRN, we obtained the UV–Vis spectra of different ACRN (Figure 4). The spectra of ACRN with different shell thicknesses exhibited plasmon resonance absorption peaks. Comparative observation showed that the plasmon resonance absorption peak gradually weakened as the amount of Ag-rGO increased. The peak at approximately 250-300 nm and 300-500 nm were assigned to the C=C and C=O bands of rGO, and the surface plasmon resonance (SPR) of the Ag decorated on rGO [27]. In addition, the peak at 500-700 nm was corresponded to the SPR of the core-shell structure, the optical absorbance increased significantly with increasing thickness of the Cu_2O nanoshell. The slight redshift of the peak at 500-700 nm was due to the increase in the local dielectric constant of Cu_2O [28].

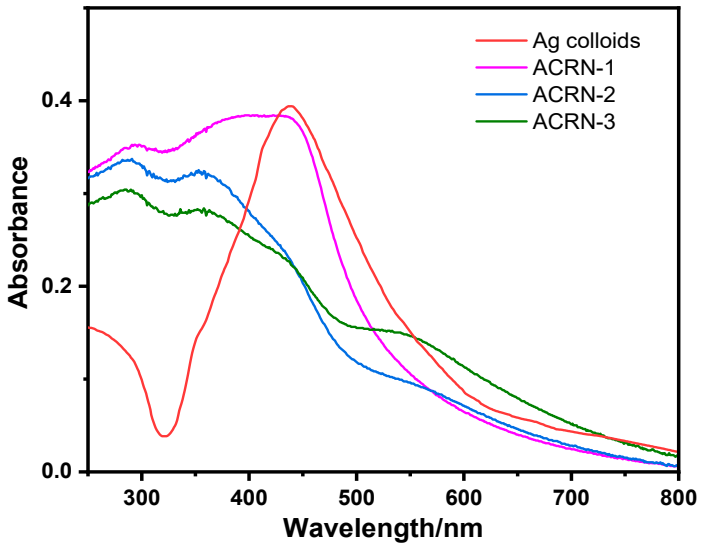

Figure 4. UV–Vis absorption spectra of Ag colloids and ACRN with different thicknesses of the Cu_2O shell.

Preprints (www.preprints.org) | NOT PEER-REVIEWED | Posted: 20 November 2023 doi:10.20944/preprints202311.1196.v1

3.2. Catalytic performance analysis

The harm of organic pollutants has received widespread attention. Developing methods to catalytically degrade these pollutants is of great importance. 4-NP was widely used in the synthesis of pesticides, drugs, and dyes, showing their potential hazards. Therefore, various catalytic materials were designed and fabricated for the reduction of it [3,4].

We employed the 4-NP as a probe molecule to evaluate the catalytic performance of ACRN. The catalytic rate for 4-NP (0.005 M) was increased significantly by adding the ACRN. We observed the absorption peak of 4-NP at approximately 320 nm (Figure 5 A-D). After the addition of $NaBH_4$, 4-NP was ionized, resulting in the red-shifted peak at approximately 400 nm (Figure 5 A-D), and the solution was changed to light yellow (Figure 1B-a). After complete degradation of 4-NP, the solution in the cuvette became colorless (Figure 1B-b), mainly due to the formation of ionic 4-NP.

In Figure 5 A-D, we observed the characteristic peak at 400 nm was gradually decreased and disappeared, and new peaks at approximately 310 nm gradually increased, indicating the generation of p-aminophenol (4-AP). As we know, the work function of Ag was smaller than Cu_2O, so electrons were transferred to Ag core from the Cu_2O shell. There was a large amount of positive charge on the surface of Cu_2O, which attracted 4-NP to the Ag@Cu_2O and accelerated BH_4^- catalytic degradation. In addition, rGO had an efficient electron transfer platform, allowing rapid electron transfer and resulting in a high catalytic efficiency.

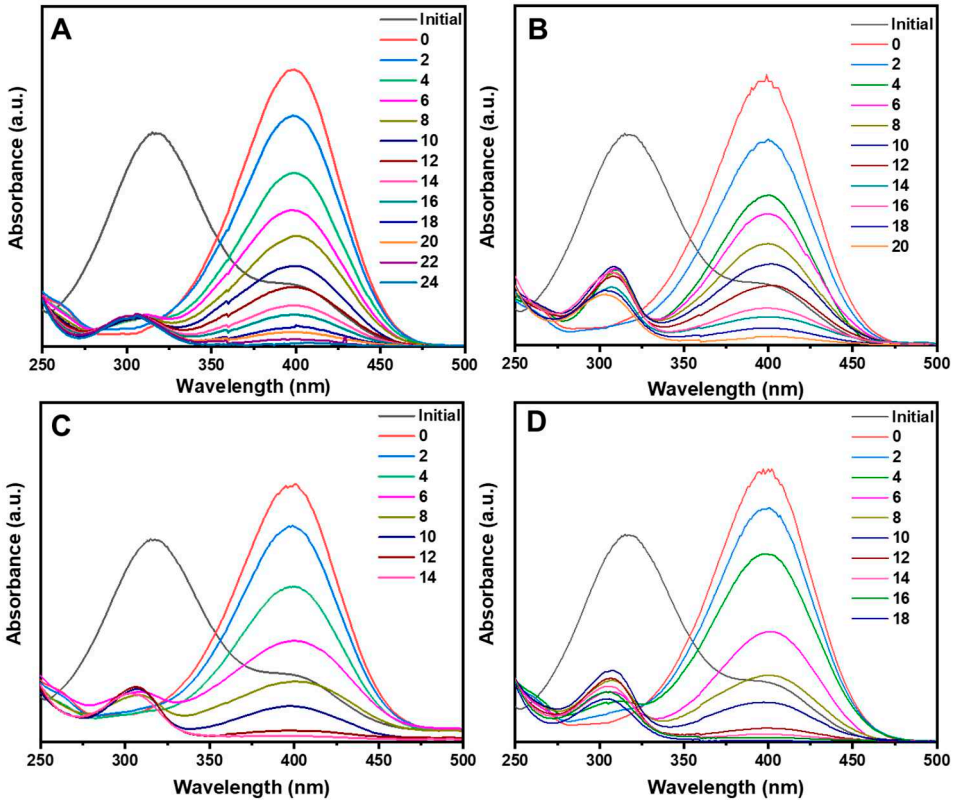

Figure 5. UV–Vis absorption spectra of the reduction of 4-NP by the introduction of (A) Ag-rGO (t = 24 min), (B) ACRN-1 (t = 20 min), (C) ACRN-2 (t = 14 min) and (D) ACRN-3 (t = 18 min).

The ACRN exhibited porous structures and provided many active sites. During the catalytic reactions, the electrons on the Ag@Cu_2O surface were transferred to BH_4^-, and 4-NP was reduced to 4-AP. As shown in Figure 5 A-D, the complete degradation of 4-NP by Ag-rGO and three different ACRN occurred in less than 24 min, indicating the excellent performance of the fabricated catalytic materials. Figure 5C indicates that the ACRN-2 exhibited the best catalytic efficiency, and the catalytic time was approximately 14 min. As shown in Figure 6, the absorption logarithm [ln (C_t/C_0)] and time (t) exhibited the linear relationship, which indicated catalytic reduction of 4-NP was related to the ACRN following a first-order kinetic relationship. The catalytic reaction rate constants for 4-NP were

Preprints (www.preprints.org) | NOT PEER-REVIEWED | Posted: 20 November 2023 doi:10.20944/preprints202311.1196.v1

0.16, 0.16, 1.29, and 0.23 min^{-1}, indicating that ACRN-2 exhibited excellent catalytic activity, as the reaction rate was proportional to the reaction rate constant.

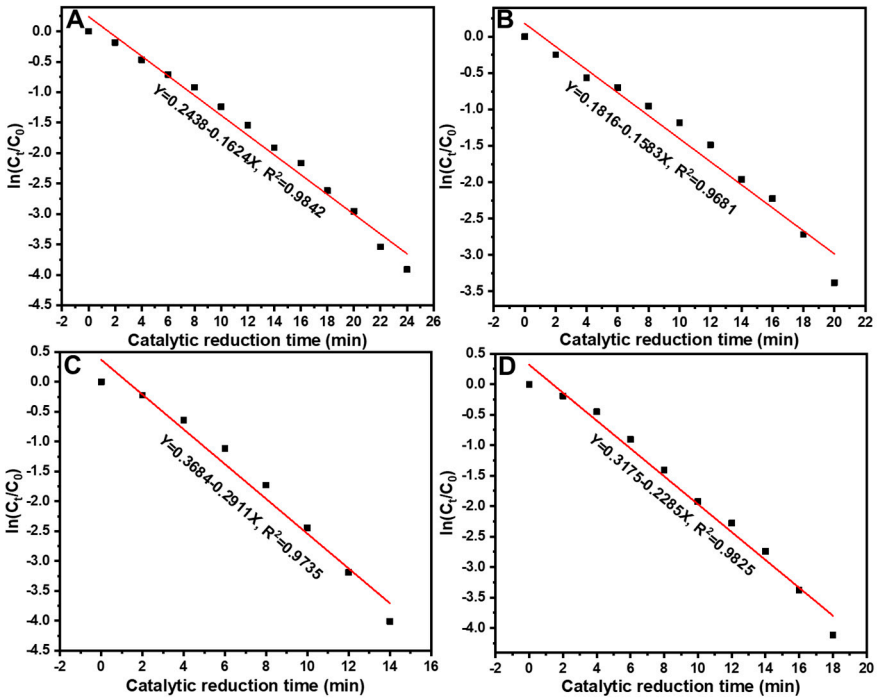

Figure 6. Logarithm of C_t/C_0 versus catalytic reduction time of (A) Ag-rGO and (B) ACRN-1, (C) ACRN-2, and (D) ACRN-3.

MO and TNP are abundant in soil and water, and the catalytic degradation of MO and TNP in water is required for environmental protection [29,30]. Therefore, the optimal ACRN-2 was utilized for the catalytic degradation of MO and TNP, which are toxic and explosive pollutants, and the catalytic process was observed by UV–Vis absorption spectroscopy (Figure 7A and 7B). The absorption peaks attributed to MO and TNP at 464 and 390 nm, respectively, gradually decreased, indicating that MO and TNP were catalytically degraded, and the ACRN-2 exhibited higher catalytic efficiency for MO than TNP. Furthermore, the linear relationship between the absorption logarithm [ln (C_t/C_0)] and time (t) in Figure 7C and 7D indicated that the reduction process of MO and TNP was associated with the ACRN-2 and followed a first-order kinetic relationship. The catalytic reaction rate constants were 0.34 and 0.08 min^{-1} for MO and TNP, respectively.

The high absorption capacity of the ACRN was due to the abundant active sites on Cu_2O that improve the catalytic performance. This also clearly indicated that the ACRN had excellent catalytic efficiency, trace catalytic activity, and high electron transfer efficiency, so the material exhibited excellent catalytic performance.

Preprints (www.preprints.org) | NOT PEER-REVIEWED | Posted: 20 November 2023 doi:10.20944/preprints202311.1196.v1

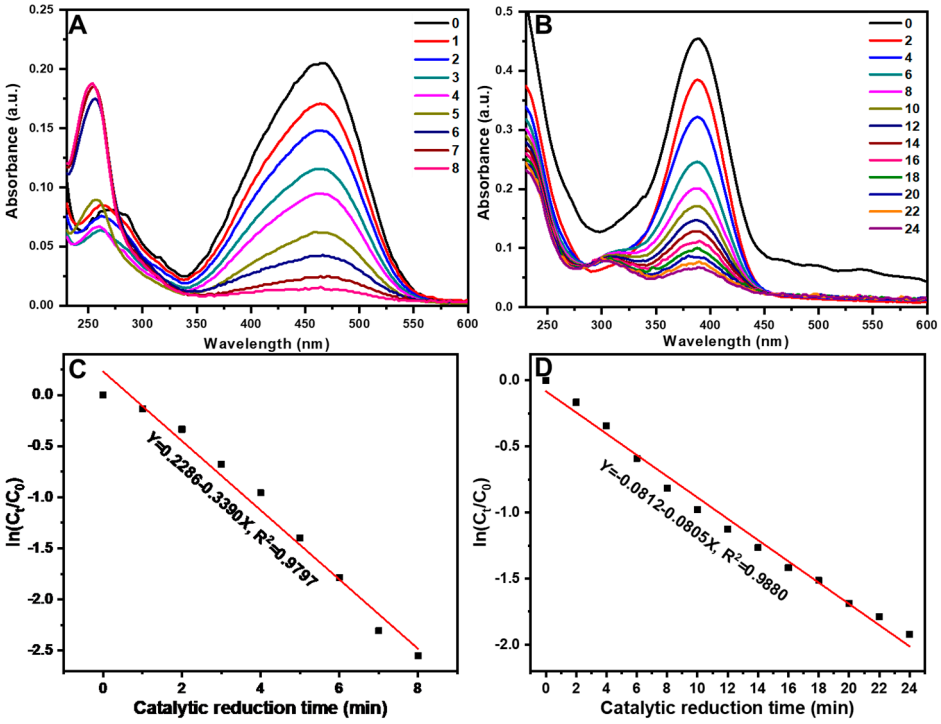

Figure 7. UV–Vis absorption spectra during the catalytic reduction of (A) MO and (B) TNP by introducing the ACRN-2. Logarithm of C_t/C_0 versus catalytic reduction time for (C) MO and (D) TNP.

4. Conclusions

To develop low-consumption and environmentally friendly organic pollutant degradation technologies, we designed ACRN for the chemical reduction of potential pollutants. The morphology and properties of the ACRN were analysized by UV–Vis spectroscopy, TEM, and SEM. To study the catalytic activity of ACRN, we selected 4-NP as a probe molecule and revealed the excellent chemical catalytic activity for the degradation of 4-NP. Notably, among the four catalytic materials with different Cu_2O shell thicknesses, the ACRN-2 exhibited excellent catalytic performance due to its superior electron transfer ability after the introduction of the rGO platform. More importantly, the fabricated ACRN exhibited excellent adsorption properties and significantly improved the degradation rate of 4-NP. Moreover, the ACRN demonstrated the potential for the improvement for reduction of phenolic pollutants. These ACRN have significant potential for applications in catalytic systems for the removal of the harmful substances from water. The graphene-based material in catalytic study is of great significance for the development of nanomaterial science.

Supplementary Materials: The following supporting information can be downloaded at the website of this paper posted on Preprints.org.

Author Contributions: writing—original draft preparation, L.C.; formal analysis, L.C.; methodology, L. C. and S.G.; data curation, E.P.; writing—review and editing, Y.M.J.; funding acquisition, Y.M.J. All authors have read and agreed to the published version of the manuscript.

Funding: This work was supported by the National Research Foundation of Korea (NRF) grants funded by the Korea government (RS-2023-00271205 and 2021R1A2C2004550) and by Korea Basic Science Institute (National Research Facilities and Equipment Center) grant funded by the Ministry of Education (2020R1A6C101A195).

Conflicts of Interest: The authors declare no conflict of interest.

References

1. Lellis, B.; Fávaro-Polonio, C.Z.; Pamphile, J.A.; Polonio, J.C. Effects of Textile Dyes on Health and the Environment and Bioremediation Potential of Living Organisms. *Biotechnol. Res. Innov.* **2019**, *3*, 275-290.
2. Hassan, M.M.; Carr, C.M. A Critical Review on Recent Advancements of the Removal of Reactive Dyes from Adsorbents, Dyehouse Effluent by Ion-Exchange. *Chemosphere* **2018**, *209*, 201-219.

3. Corma, A.; Serna, P. Chemoselective hydrogenation of nitro compounds with supported gold catalysts. *Science* **2006**, *313*, 332–334.
4. Sekler, M.S.; Levi, Y.; Polyak, B.; Novoa, A.; Dunlop, P.S.M.; Byrne, J.A.; Marks, R.S. Monitoring genotoxicity during the photocatalytic degradation of p-nitrophenol. *J. Appl. Toxicol.* **2004**, *24*, 395–400.
5. Song, J.J.; Huang, Z.F.; Pan, L.; Li, K.; Zhang, X.W.; Wang, L.; Zou, J.J. Review on selective hydrogenation of nitroarene by catalytic, photocatalytic and electrocatalytic reactions. *Appl. Catal. B-Environ.* **2018**, *227*, 386–408.
6. Eichenbaum, G.; Johnson, M.; Kirkland, D.; O'Neill, P.; Stellar, S.; Bielawne, J.; DeWire, R.; Areia, D.; Bryant, S.; Weiner, S.; Desai-Krieger, D.; Guzzie-Peck, P.; Evans, D.C.; Tonelli, A. Assessment of the genotoxic and carcinogenic risks of pnitrophenol when it is present as an impurity in a drug product. *Regul. Toxicol. Pharmacol.* **2009**, *55*, 33–42.
7. Liu, R.; Mahurin, S.M.; Li, C.; Unocic, R.R.; Idrobo, J.C.; Gao, H.; Pennycook, S.J.; Dai, S.; Dopamine as a Carbon Source: The Controlled Synthesis of Hollow Carbon Spheres and Yolk-Structured Carbon Nanocomposites. *Angew. Chem. Int. Ed.* **2011**, *50*, 6799-6802.
8. Zhou, M.; Wei, X.; Zhang, X.; Gao, X.; Wang, X.; Wu, W.D.; Selomulya, C.; Wu, Z. Uniform mesoporous carbon hollow microspheres imparted with surface-enriched gold nanoparticles enable fast flow adsorption and catalytic reduction of nitrophenols. *J. Colloid Interface Sci.* **2019**, *537*, 112-122.
9. Ghiat, I.; Saadi, A.; Bachari, K.; Coville, N. J.; Boudjemaa, A. Catalytic reduction of 4-nitrophenol to 4-aminophenol over Ni/SiO_2 catalyst made from reduced SiO_2@NiPhy. *Res. Chem. Intermediat.* **2023**, *49*, 4349–4365.
10. Huang, S.C.; You, Z.X.; Jhang, S.M.; Lin, C.Y. Facile electrochemical preparation of NiFeP submicron-spheres as an efficient electrocatalyst for the electrochemical hydrogenation of 4-nitrophenol at neutral pH. *J. Environ.l Chem. Eng.* **2022**, *10*, 108882.
11. Suchomel, P.; Kvitek, L.; Prucek, R.; Panacek, A.; Halder, A.; Vajda, S.; Zboril, R. Simple size-controlled synthesis of Au nanoparticles and their size-dependent catalytic activity. *Sci. Rep.* **2018**, *8*, 4589.
12. Chen, X.; Cai, Z.; Chen, X.; Oyama, M. AuPd bimetallic nanoparticles decorated on graphene nanosheets: Their green synthesis, growth mechanism and high catalytic ability in 4-nitrophenol reduction. *J. Mater. Chem. A* **2014**, *2*, 5668–5674.
13. Teimouri, M.; Khosravi-Nejad, F.; Attar, F.; Saboury, A.A.; Kostova, I.; Benelli, G.; Falahati, M. Gold nanoparticles fabrication by plant extracts: Synthesis, characterization, degradation of 4-nitrophenol from industrial wastewater, and insecticidal activity—A review. *J. Clean. Prod.* **2018**, *184*, 740–753.
14. Feng, L.; Gao, G.; Huang, P.; Wang, K.; Wang, X.; Luo, T.; Zhang, C. Optical properties and catalytic activity of bimetallic gold-silver nanoparticles. *Nano Biomed. Eng.* **2010**, *2*, 258–267.
15. Gregory, J.W.; Gong, Y.; Han, Y.; Huband, S.; Walton, R.I.; Hessel, V.; Rebrov, E.V. Au/TiO_2 coatings for photocatalytic reduction of 4-nitrophenol to 4-aminophenol with green light. *Catal. Today* **2023**, *418*, 114145.
16. Shang, Z.; Yang, Z.; Xiao, Y.; Wang, X. Ordered mesoporous Ag/CeO_2 nanocrystalline via silica-templated solution combustion for enhanced photocatalytic performance. *Colloid. Surface. A* **2020**, *604*, 125301.
17. Shaik, M.R.; Adil, S.F.; Kuniyil, M.; Sharif, M.; Al-Warthan, A.; Siddiqui, M.R.H.; Ali, M. I.; Tahir M.N.; Khan, M. Facile Sonochemical Preparation of Au-ZrO_2 Nanocatalyst for the Catalytic Reduction of 4-Nitrophenol. *Appl. Sci.* **2020**, *10*, 503.
18. Đurasović, I.; Štefanić, G.; Dražić, G.; Peter, R.; Klencsár, Z.; Marciuš, M.; Jurkin, T.; Ivanda, M.; Stichleutner S.; Gotić, M. Microwave-Assisted Synthesis of Pt/SnO_2 for the Catalytic Reduction of 4-Nitrophenol to 4-Aminophenol. *Nanomaterials* **2023**, *13*, 2481.
19. Li, F.; Liu, Y.; Ma, T.; Xu, D.; Li, X.; Gong, G. Catalysis of the hydro-dechlorination of 4-chlorophenol and the reduction of 4-nitrophenol by Pd/Fe_3O_4@C. ***New J. Chem.*** **2015**, ***39***, 6474-6481.
20. Chen, L.; Liu, M.; Zhao, Y.; Kou, Q.; Wang, Y.; Liu, Y.; Zhang, Y.; Yang, J.; Jung, Y.M. Enhanced catalyst activity by decorating of Au on Ag@Cu_2O nanoshell. *Appl. Surf. Sci.* **2018**, *435*, 72–78.
21. Chen, L.; Guo, S.; Dong, L.; Zhang, F.; Gao, R.; Liu, Y.; Wang, Y.; Zhang, Y. SERS effect on the presence and absence of rGO for Ag@Cu_2O core-shell. *Mat. Sci. Semicon. Proc.* **2019**, *91*, 290–295.
22. Xu, L.; Zhang, F.; Song, X.; Yin, Z.; Bu, Y. Construction of reduced graphene oxide-supported Ag-Cu_2O composites with hierarchical structures for enhanced photocatalytic activities and recyclability. *J. Mater. Chem. A* **2015**, *3*, 5923–5933.
23. Novoselov, K.S.; Geim, A.K.; Morozov, S.V. Electric field effect in atomically thin carbon films. *Science* **2004**, *306*, 666–669.
24. Yury, G. Transition metal carbides go 2D Nature Nanotechnology. *Nat. Mater.* **2015**, *14*, 1079–1080.
25. Guo, S.J.; Dong, S.J. Graphene nanosheet: synthesis, molecular engineering, thin film, hybrids, and energy and analytical applications, *Chem. Soc. Rev.* **2011**, *40*, 2644–2672.
26. Huang, X.; Qi, X.Y.; Boey, F.; Zhang, H. Graphene-based composites. *Chem. Soc. Rev.* **2012**, *41*, 666–686.
27. Xiong, X.; Li, L.; Chen, J.; Zhang, S.; Wang, L.; Dou, S. Facile synthesis of highly efficient one-dimensional plasmonic photocatalysts through Ag@Cu_2O core-shell hetero-nanowires. *ACS Appl. Mater. Interfaces* **2014**, *6*, 15716–15725.

28. Guo, S.; Wang, Y.; Zhang, F.; Gao, R.; Liu, M.; Dong, L.; Liu, Y.; Zhang, Y. Chen, L. In Situ Synthesis of Ag@Cu_2O-rGO Architecture for Strong Light-Matter Interactions**.** *Nanomaterials* **2018**, *8*, 444.
29. Lu, Q.; Wei, Z.; Li, C.; Ma, J.; Li, L. Photocatalytic degradation of methyl orange by noble metal Ag modified semiconductor Zn_2SnO_4. *Mat. Sci. Semicon. Proc.* **2022**, *138*, 106290.
30. Kayser, E.G.; Burlinson N.E. Migration of explosives in soil: analysis of rdx, tnt, and tetryl from a 14c lysimeter study. *J. Energy. Mater.* **1988**, *6*, 45-71.